Progress In Electromagnetics Research, PIER 32, 357–381, 2001

FREQUENCY DOMAIN ANALYSIS OF WAVEGUIDES AND RESONATORS WITH FIT ON NON-ORTHOGONAL TRIANGULAR GRIDS

U. van Rienen

Institute of General Electrical Engineering
Faculty of Engineering, Rostock University
D-18051 Rostock, Germany

Abstract—The focus of this paper is on the solution of Maxwell's equations for time-harmonic fields on triangular, possibly non-orthogonal meshes. The method is based on the well-known Finite Integration Technique (FIT) [33, 35] which is a proven consistent discretization method for the computation of electromagnetic fields. FIT on triangular grids was first introduced in [29, 31] for eigenvalue problems arising in the design of accelerator components and dielectric loaded waveguides. For many technical applications the 2D simulation on a triangular grid combines the advantages of FIT, as e.g. the consistency of the method or the numerical advantage of banded system matrices, with the geometrical flexibility of non-coordinate grids. The FIT-discretization on non-orthogonal 2D grids has close relations [26] to the Nédélec elements [14, 15] or edge elements in the Finite Element Method.

1. INTRODUCTION

The most important class of methods for numerical field calculation deals with local difference equations obtained after suitable discretization. Well-known examples are the Finite Difference Method (FD) and the Finite Element Method (FEM). The Finite Integration Technique [33, 35, 36], shortly FIT, presents a discretization consistent with Maxwell's equations, i.e., the resulting discrete solutions reflect the analytical properties of the continuous solutions. The Finite Integration Technique can best be described as a Finite Volume method. It has been developed specifically for the solution of Maxwell's equations. The goal of this development was the ability to solve numerically the complete system of Maxwell's equations in full generality.

Regard Maxwell's equations which can either be written in integral form or in differential form

$$\begin{aligned}
\oint_{\partial A} \vec{E} \cdot d\vec{s} &= -\int_A \frac{\partial \vec{B}}{\partial t} \cdot d\vec{A} &\iff \quad \operatorname{curl} \vec{E} &= -\frac{\partial \vec{B}}{\partial t} \\
\oint_{\partial A} \vec{H} \cdot d\vec{s} &= \int_A (\frac{\partial \vec{D}}{\partial t} + \vec{J}) \cdot d\vec{A} &\iff \quad \operatorname{curl} \vec{H} &= \frac{\partial \vec{D}}{\partial t} + \vec{J} \\
\oint_{\partial V} \vec{D} \cdot d\vec{A} &= \int_V \rho \cdot dV &\iff \quad \operatorname{div} \vec{D} &= \rho \\
\oint_{\partial V} \vec{B} \cdot d\vec{A} &= 0 &\iff \quad \operatorname{div} \vec{B} &= 0
\end{aligned}$$

where A is any given surface and V any given volume.

The Finite Integration Technique yields an *exact* representation of Maxwell's equations in integral form onto a grid duplet $(G, \tilde{G})$. The FIT grid duplet $(G, \tilde{G})$ is not coordinate-bounded, not necessarily orthogonal, not necessarily regular. Yee's FDTD-method [40] (1966) with the "Leap Frog"-scheme is a predecessor of FIT in Finite Difference Time Domain (FDTD stands for *Finite Difference Time Domain*). The feature of Yee's method is that it evaluates Maxwell's equations for *both* electromagnetic fields (not just the electric field) and

that the electric and magnetic field components were allocated on two staggered grids. In 1977, Weiland [33] generalized the FDTD-method to a general numerical method for all electrodynamics. In fact, FIT is not restricted to electrodynamics only but is also a suitable numerical method for other subjects. For example, FIT was recently applied in acoustics [39], elastodynamics [12, 2] and temperature problems [17, 16] and for coupled problems [28, 1].

The Finite Integration Technique makes only some usual idealizations concerning the materials: The materials of the given objects have to be *piecewise* linear, homogeneous, and isotropic so that the subdomains with constant material parameters $(\varepsilon, \mu, \kappa)$ are at least as big as the elementary volumes used.

The discretization of Maxwell's equations, i.e., the field computation in a finite number of discrete points, gives a decomposition of the solution space into grid cells. The first step towards that goal is to define a finite volume Ω, the calculation domain. Now, cover Ω with a grid G. As an example, we can consider a simple Cartesian coordinate grid. It has to be stressed at this point, however, that a FIT grid G is defined in much more generality and that its definition also includes non-coordinate grids as well as non-orthogonal grids (cf. section 2 and [31, 27] or e.g. [9, 10, 23, 20, 21]). For the simple Cartesian coordinate grid, we will explain very briefly the derivation of the Maxwell Grid Equations. Further details can be found e.g. in [37, 6, 27].

DEFINITION 1. *A FIT grid G is defined as:*
- $G \in \mathbf{R}^3$ $(\mathbf{R}^2)$ *simply connected*
- *elementary volumes* $V = \{V_1, ..., V_{n_V}\}$ *with* $G = \bigcup V_i,\ V_i \neq \{\}$;
- *elementary areas* $A = \{A_1, ..., A_{n_A}\}$ *with* $\{A_i\} := \bigcap V_i$
- *elementary lines* $L = \{L_1, ..., L_{n_L}\}$ *with* $\{L_i\} := \bigcap A_i$
- *(grid) points* $P = \{P_1, ..., P_{n_P}\}$ *with* $\{P_i\} := \bigcap L_i$

An elementary volume V_i (FIT cell) for the simplest case is shown in Fig. 1. Next, state variables [34] are introduced on the grid G:

DEFINITION 2. *The electric (grid-)voltage* $e_i := \int_{L_i} \vec{E} \cdot d\vec{s}$ *is assigned to each elementary line* L_i *as state variable.*
The magnetic (grid-)flux $b_i := \int_{A_i} \vec{B} \cdot d\vec{A}$ *normal to the elementary area* A_i *is assigned as state variable to each elementary area* A_i.

After appropriate numbering of the points of the grid, the state variables e_i and $b_i,\ i = 1, \ldots, 3N$ can be stored in vectors e and b and

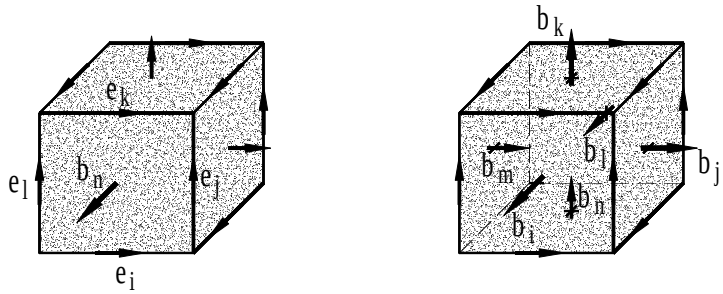

Figure 1. Elementary volume of a Cartesian FIT grid G with the allocated state variables *electric grid voltage* (left) and *magnetic grid flux* (right).

a discrete form of the induction law can be deduced:

$$Ce = -\frac{\partial}{\partial t} b.$$

The $(3N \times 3N)$-matrix C, which is denoted as *discrete curl operator*, reflects the topology of the grid. Actually, for a Cartesian grid with lexicographic numbering the matrix C is a block matrix with blocks $\pm P_x, \pm P_y, \pm P_z$ and 0:

$$C = \begin{pmatrix} 0 & -P_z & P_y \\ P_z & 0 & -P_x \\ -P_y & P_x & 0 \end{pmatrix},$$

where x, y, z are the three coordinate directions. The blocks P_x, P_y, P_z each have -1's on their main diagonal and 1's on some sub- or (super-)diagonal the distance of which to the main diagonal agrees with the chosen numbering. On *dual-orthogonal* Cartesian FIT grids ($G \perp \tilde{G}$, cf. Def. 1) we have:

$$P_x \simeq \frac{\partial}{\partial x},\ P_y \simeq \frac{\partial}{\partial y},\ P_x \simeq \frac{\partial}{\partial x}.$$

For cylindrical symmetric structures the curl operator for a triangular 2D grid will be given in section 2, that one for a cylindrical 3D grid can be found in [9].

Using the vector b again and introducing a matrix S of size $N \times 3N$ with elements $\{-1, 1\}$ corresponding to the topology of the grid:

$$S := (P_x | P_y | P_z).$$

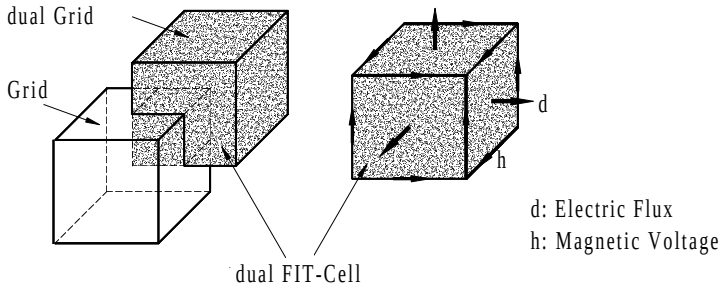

Figure 2. Elementary volume of the dual grid $\tilde{G}$ for the Cartesian FIT grid G and the allocated state variables *magnetic grid voltage* and *electric grid flux*.

So, the discrete form of the divergence equation is

$$Sb = 0.$$

It remains to transfer the second and third Maxwell's equations. This will be completely analogous to the transfer of the first and fourth Maxwell's equations. For that, the so-called dual grid $\tilde{G}$ is introduced. For a Cartesian grid, it equals the grid G shifted by half a cell length. Again, the definition of the dual FIT grid is much more general than what example may suggest (cf. sect. 2 or e.g. [21]).

DEFINITION 3. *The dual FIT grid $\tilde{G}$ can be formally described as*
- *$\tilde{G}$ as G with $\tilde{V}, \tilde{A}, \tilde{L}, \tilde{P}$*
- *$\forall \tilde{V}_j \; \exists P_i$ with $P_i \in \tilde{V}_j$, $\forall V_j \; \exists \tilde{P}_i$ with $\tilde{P}_i \in V_j$*
- *$\forall \tilde{A}_j \; \exists L_i$ with $L_i \bigcap \tilde{A}_j \neq \{\}$, $\forall A_j \; \exists \tilde{L}_i$ with $\tilde{L}_i \bigcap A_j \neq \{\}$.*

The dual-orthogonal FIT grid is defined by the relations $L \perp \tilde{A}$ and $\tilde{L} \perp A$.

The state variables h and d are introduced analogously to e and b:

DEFINITION 4. *The magnetic voltage h_i is assigned as state variable to each dual elementary line $\tilde{L}_i$: $h_i := \int_{\tilde{L}_i} \vec{H} \cdot d\vec{s}$.*
The electric flux d_i normal to the dual grid surface $\tilde{A}_i$ is assigned as state variable to each dual elementary area $\tilde{A}_i$: $d_i := \int_{\tilde{A}_i} \vec{D} \cdot d\vec{A}$.
Furthermore, the total electric current j_i normal to the dual grid surface $\tilde{A}_i$ is assigned as state variable to each dual elementary area

$\tilde{A}_i$: $j_i := \int_{\tilde{A}_i} \vec{J} \cdot d\vec{A}$.
The discrete charges q_i (allocated in P_i on G) are assigned as state variables to each dual elementary volume $\tilde{V}_i$: $q_i := \int_{\tilde{V}_i} \rho dV$.

The values of the state variables are stored in topological matrices $\tilde{C}$ and $\tilde{S}$ analogous to C and S. Thus, the discrete form of Ampere's law is

$$\tilde{C}h = \frac{\partial}{\partial t} d + j$$

and Coulomb's law is

$$\tilde{S}d = q.$$

To summarize the above, let us formally define the Maxwell Grid Equations. It should be emphasized that no approximations have been made so far. Only when the material equations are transferred to the grid space, FIT will require some approximations.

$$\begin{aligned} Ce &= -\dot{b} \\ \tilde{C}h &= \dot{d} + j \\ Sb &= 0 \\ \tilde{S}d &= q \end{aligned} \tag{1}$$

Because of its consistency and generality this system is denoted as *Maxwell-Grid-Equations*. The operators C, $\tilde{C}$, S and $\tilde{S}$ can be interpreted as discrete curl operators $C, \tilde{C}$, discrete divergence $S, \tilde{S}$ and discrete gradient operators $-S^T, -\tilde{S}^T$. The characteristics of the Finite Integration Technique are not given here. They can be found in [38, 11, 5] or [27].

Until now, no approximations have been used at all. They will be necessary after the transfer of the material equations to the grid space. The state variables d_i and e_i (respectively b_i and h_i) are each allocated at the same points. There is an analogue of the material equations relating them to each other. In order to find that analogue of the material equations, the grid flux is divided by the grid voltage. The ratios d_i/e_i and b_i/h_i (j_i/e_i, respectively) then will be approximated by averaging the corresponding material parameters. The averaged quantities are then combined in the so-called *material matrices* $D_\varepsilon, \tilde{D}_\mu$ and D_κ. A detailed description of this approximation can be found in [9, 6, 37]. We follow the formulation in [9]:

Definition 5. *The elementary areas A_i and the corresponding dual elementary lines $\tilde{L}_i$ shall each be coordinate planes resp. coordinate*

lines of a local orthogonal coordinate system which is differentiable twice with respect to its Cartesian representation. The dual grid line $\tilde{L}_i$ intersects the area A_i in its local middle point and vice versa. The permeability operator is then given by

$$\tilde{D}_{\mu,i} = \frac{\int_{L_m} \int_{L_n} dA}{\int_{\tilde{L}_i} \frac{1}{\mu} ds}.$$

The (dual) elementary areas $\tilde{A}_i$ and the corresponding elementary lines L_i shall each be coordinate planes resp. coordinate lines of a local orthogonal coordinate system which is differentiable twice with respect to its Cartesian representation. The grid line L_i intersects the area $\tilde{A}_i$ in its local middle point and vice versa. The permittivity operator is then given by

$$D_{\varepsilon,i} = \frac{\int_{\tilde{L}_m} \int_{\tilde{L}_n} \varepsilon dA}{\int_{L_i} ds}.$$

Thus, the construction of $\tilde{D}_{\mu,i}$ is based on lengthwise averaging. Its error is linear with respect to the energy norm if A_i represents a border of different permeabilities, otherwise it is quadratic. The construction of $D_{\varepsilon,i}$ is based on areawise averaging. Its error is linear with respect to the energy norm if L_i borders different permittivities or permeabilities, otherwise it is quadratic.

Defining the conductivity operator D_κ in analogy, thus the following transfer of the electromagnetic material equations to the grid space results with diagonal material operators $D_\varepsilon, \tilde{D}_\mu, D_\kappa$:

$$\begin{array}{rclcrcl} \vec{D} & = & \varepsilon \vec{E} & \rightarrow & d & = & D_\varepsilon e \\ \vec{B} & = & \mu \vec{H} & \rightarrow & b & = & \tilde{D}_\mu h \\ \vec{J}_L & = & \kappa \vec{E} & \rightarrow & j_l & = & D_\kappa e \end{array}$$

Finally, boundary equations at ∂G are needed. Dirichlet and Neumann boundary conditions can be implemented in a FIT-scheme in a very natural way, others like open (absorbing), periodic or waveguide boundary conditions have also been realized (see e.g. [37, 9, 5]).

Non-coordinate and non-orthogonal meshes offer an enhanced flexibility with regard to the spatial discretization of the field equations. Here, with a "coordinate mesh" a mesh is meant where the grid planes are coordinate planes in one of the usual coordinate systems as e.g. the Cartesian or cylindrical coordinate system. The triangular grids which are subject of this paper are an example for a "non-coordinate mesh". In the eighties when mainframes were the computers at hand allowing

only for very limited storage space and computing time for a single simulation the advantage of a non-coordinate, even non-orthogonal grid was of great importance because it allowed for a good approximation of shapes which posed problems for coordinate grids as e.g. a Cartesian grid. This was the main motivation to develop an automatic mesh generator for a triangular FIT grid with hexagonal dual grid. This mesh generator is the kernel of the resonator and waveguide program URMEL-T [31] while its predecessor URMEL [33] used Cartesian grids.

2. FIT-DISCRETIZATION ON A TRIANGULAR GRID

In the previous section the *Maxwell-Grid-Equations* (1) were generally defined. Now the characteristics of a triangular FIT grid will be shown and some discrete quantities as the state variables, operators, etc., will be given. As in the usual Finite Difference Methods, FIT solves Maxwell's equations on a domain Ω which holds the actual solution domain Ω_s as a sub-domain: $\Omega = \Omega_s \cup \Omega_o$. The domain Ω_s may again be composed of several sub-domains, holding e.g. different material. Discretization on Ω rather than on Ω_s has the advantage of allowing for higher topological regularity. With adequate numbering scheme this, in consequence leads to matrices with regular (band) pattern which pays off by a speed up in the solution process of the linear algebraic problems (e.g. by faster matrix-vector multiplications).

Often the solution domain Ω_s possesses symmetries or some geometrical invariance such that the 3D problem may be reduced to a 2D problem by appropriate variable separation. For example, this is the case for cavities with circular cylindrical symmetry or for longitudinally invariant waveguides [33, 31]. The 2D domain shall now be covered by a triangular grid. This mesh has the advantage to approximate well also curved boundaries - even for relatively coarse grids (see Fig. 3).

2.1. The Triangular Grid and its Dual Grid

Without loss of generality it is assumed that the electric voltages are allocated on the triangular grid G and the magnetic voltages on the dual grid $\tilde{G}$ (see [31] for special details on the alternative allocation). The two cases of an orthogonal and a non-orthogonal grid duplet will both be treated:
(i) *Orthogonal case*:
An orthogonal dual grid composed of the perpendicular bisectors of the elementary lines L_i is chosen if all triangles of the grid inside Ω_s are acute or right-angled, (see Fig. 4). The intersections of the

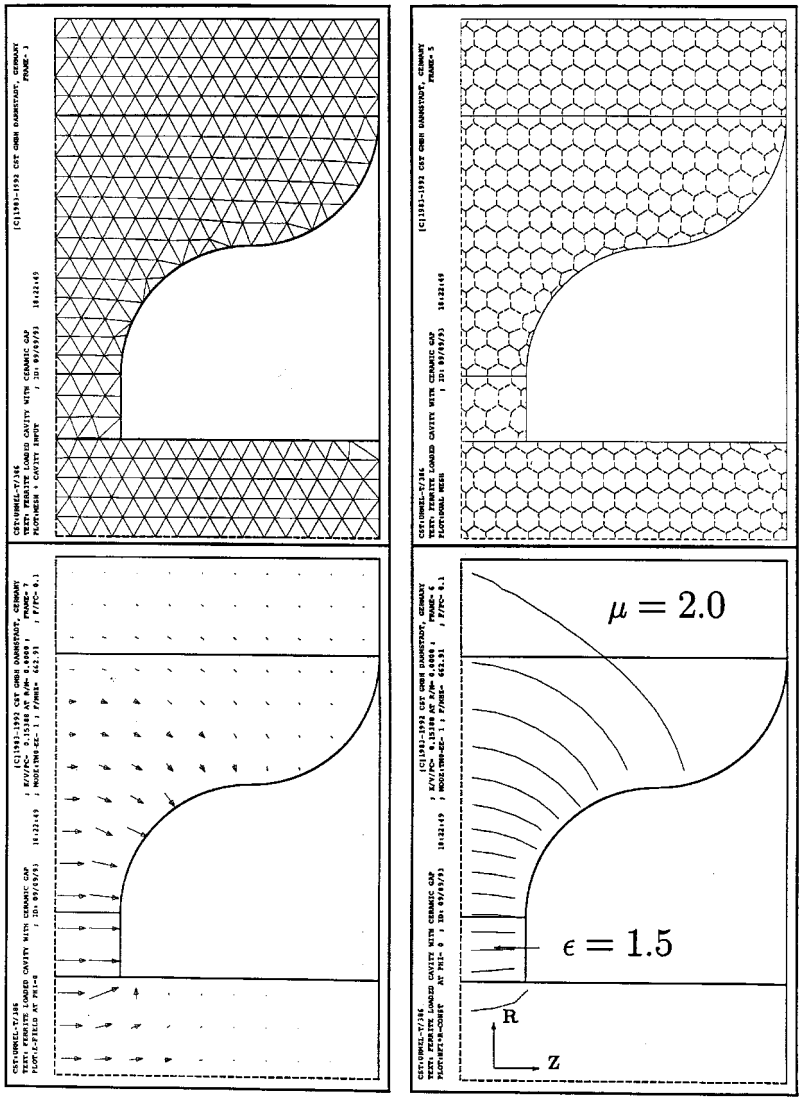

Figure 3. Two-dimensional triangular grid and computed fields for a cylindrically symmetric structure (cavity filled with ferrite and ceramics). Only the right half of the resonator is discretized applying a symmetry condition at the left boundary. The illustration on the top left shows the triangular grid G, in the top right-hand corner the corresponding dual grid $\tilde{G}$ is shown. Down on the left the electric field $\vec{E}$ is displayed, down on the right the isometric lines of $H_\varphi \cdot r$ are shown.

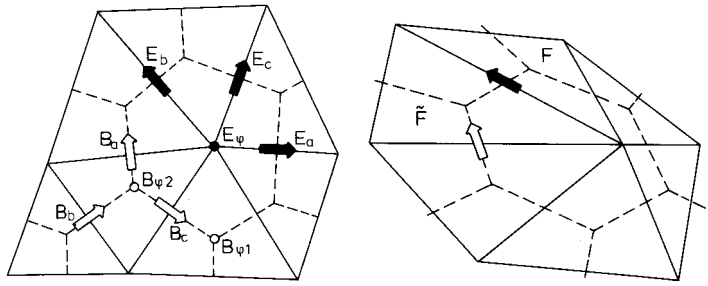

Figure 4. Left: Triangular mesh and its dual (hexagonal) mesh $\tilde{G}_{\perp}$. Right: Dual mesh $\tilde{G}_{\natural}$ with centers of mass as mesh points. Here $(F, \tilde{F})$ represent either $(\vec{E}, \vec{B})$ or $(\vec{H}, \vec{D})$.

perpendicular bisectors give the dual grid points $\tilde{P}_i$ (which are just the centers of the triangles' circumcircles). This dual mesh is denoted as $\tilde{G}_{\perp}$. Its elementary areas $\tilde{A}_i$ are general hexagons.

Note that this kind of grid is often denoted as Delaunay-Voronoi mesh in the context of Finite Element Methods.

(ii) *Non-orthogonal case*:

The automatic mesh generator starts with regular triangles and moves the grid points P_i aiming for a good approximation of the boundary $\partial\Omega_s$ resp. boundaries $\partial\Omega_{s_i}$ for $\Omega_s = \cup_i \Omega_{s_i}$. This process cannot always avoid obtuse triangles. In this case we use the centers of mass as dual mesh points thus avoiding dual mesh points outside the proper triangles (see Fig. 4). This dual mesh is denoted as $\tilde{G}_{\natural}$. Its elementary areas $\tilde{A}_i$ are hexagons, too.

With $(G, \tilde{G}_{\natural})$ the approximation order reduces to first order which is the reason why it is not generally used in URMEL-T. In most cases it suffices to increase the number of mesh points in order to avoid the use of the non-orthogonal mesh and thus the reduction in approximation order.

(iii) *Combined dual grid*:

Aiming to keep the reduction of approximation order as localized as possible, URMEL-T in fact does offer a third possibility which is a combination of $\tilde{G}_{\perp}$ and $\tilde{G}_{\natural}$: Perpendicular bisectors are used to build the dual mesh wherever this is possible and only in the (usually very few) obtuse triangles the centers of mass are used as dual mesh points.

Note that there is a great similarity to simplicial meshes with barycentric subdivisions as used in Finite Elements Methods (see also [26, 27]). Yet, the difference is that the centers of mass are connected by some straight line in $\tilde{G}_{\natural}$ while this is not necessarily the case in

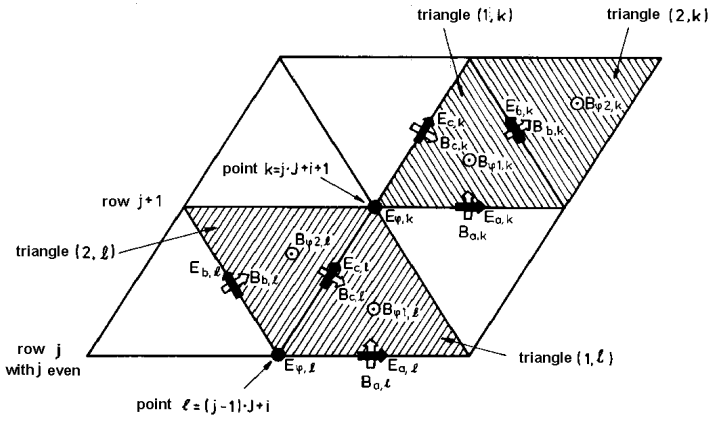

Figure 5. Location of the field components and the triangles associated with one mesh point.

simplicial meshes with barycentric subdivisions (see e.g. [22]).

The mesh points are numbered in lexicographic order. There are two kinds of triangles alternating in the rows: One has the vertex on top, while the other one is standing upright. One of each kind is associated with each mesh point k [$k = (j-1) \cdot J + i$ with $j = 1, ..., J, i = 1, ..., I$]. The triangle of the first kind is named (1,k) and the second (2,k). A point $k = (j-1) \cdot J + i$ in row j with even j is denoted as of 'type I', while a point k in row j with odd j is denoted as of 'type II'. The allocation of all the field components, associated with a mesh point, is illustrated in Fig. 5 for the points l of type I and k of type II.

2.2. Continuity Conditions for the Non-Orthogonal Case

The permittivity and the permeability shall be real. For $\tilde{G}_\perp$ as dual grid, any inserted material may have different μ_r and ϵ_r and either the electric field $\vec{E}$ or the magnetic field $\vec{H}$ could be chosen on G. Figure 6 shows that only continuous components (i.e. $\vec{E}_\parallel$ and $\vec{B}_\perp$ resp. $\vec{H}_\parallel$ and $\vec{D}_\perp$) occur at the triangle's boundaries. So, triangles of G may be filled with any material, varying from triangle to triangle. This is just the general property for dual-orthogonal FIT grids that the continuity of $\vec{E}_\parallel$ and $\vec{B}_\perp$ on boundaries of different materials is preserved.

In the non-orthogonal case, i.e. if the dual grid $\tilde{G}_\natural$ is used in subdomains of Ω_s, we have to place the following restriction to assure the continuity of the field components:

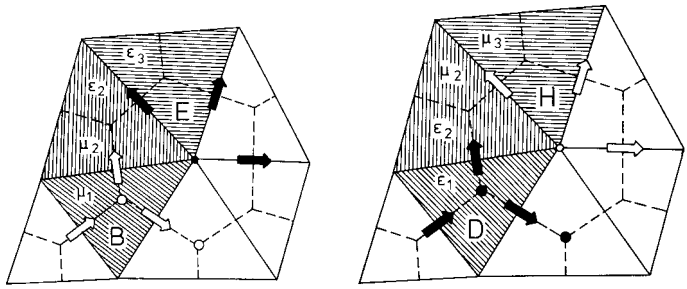

Figure 6. Material filling on grid duplet $(G, \tilde{G}_\perp)$: Either $(\vec{E},\ \vec{B})$ or $(\vec{H},\ \vec{D})$ with different μ_r, ϵ_r in both cases.

In case of electric grid voltages on G and magnetic grid fluxes on $\tilde{G}_\natural$ only material insertions with constant μ_r and arbitrary ϵ_r are allowed in those subdomains of Ω_s where the dual elementary lines $\tilde{L}_m$ are non-orthogonal to L_i. In case of magnetic grid voltages on G and electric grid fluxes on $\tilde{G}_\natural$ the material in the subdomain has to have constant ϵ_r but μ_r may vary from cell to cell. As already pointed out, for most structures it is possible to find a triangular grid G which renders $\tilde{G}_\perp$ possible as dual grid.

2.3. State Variables and Discrete Operators for the Triangular Grid

We assume that Ω_s is either cylindrically symmetric or longitudinally invariant. In this case, a variable separation is possible for either the azimuthal or the longitudinal coordinate. Furthermore, it is assumed that the fields are time-harmonic such that a description by a Fourier series is possible. Finally, the materials are assumed loss free, i.e. ϵ, μ are real and the conductivity is equal to zero. So we may write

$$\vec{E} = \sqrt{Z_0} \sin \omega t \vec{E}' \tag{2}$$

$$\vec{H} = \sqrt{Y_0} \cos \omega t \vec{H}' \tag{3}$$

with $Z_0 = \sqrt{\mu_0/\epsilon_0}$, $Y_0 = \sqrt{\epsilon_0/\mu_0}$, $c = 1/\sqrt{\mu_0 \epsilon_0}$. With the given assumptions, the electromagnetic fields can be written as:

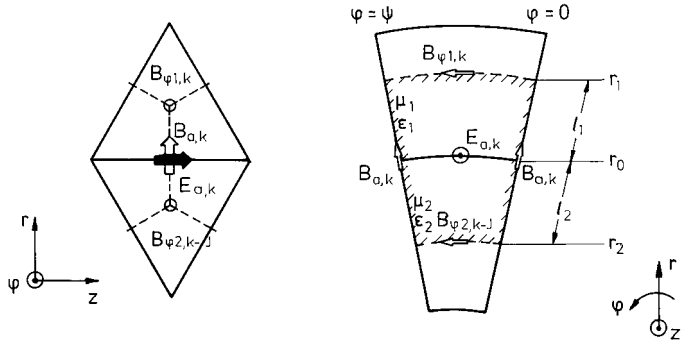

Figure 7. Integration area for the surface integral $\int_{\tilde{A}_k} \vec{E}' \cdot d\vec{A}$ for the state variable $e'_{a,k}$. Left: The section of the triangular grid is shown for better orientation of the reader. Right: The shaded area is used for integration.

$$\vec{E}'(r,\varphi,z,t) =$$
$$\sum_{m=0}^{\infty} \left[E'_{m,r}(r,z)\cos m\varphi\,\vec{e}_r + E'_{m,\varphi}(r,z)\sin m\varphi\,\vec{e}_\varphi + E'_{m,z}(r,z)\cos m\varphi\,\vec{e}_z\right].$$
$$\vec{H}'(r,\varphi,z,t) =$$
$$\sum_{m=0}^{\infty} \left[H'_{m,r}(r,z)\sin m\varphi\,\vec{e}_r + H'_{m,\varphi}(r,z)\cos m\varphi\,\vec{e}_\varphi + H'_{m,z}(r,z)\sin m\varphi\,\vec{e}_z\right].$$

in the cylindrical symmetric case, expressing the periodicity with period 2π in the azimuthal variable φ. Then we can solve Maxwell's equations for each azimuthal mode number m separately.

The grid is assumed to lie in the (r,z)-plane with $\varphi = \psi/2$ with an arbitrary[1] angle ψ. To carry over the contour, surface and volume integrals of Maxwell's equations we actually allocate $E_{a,k}, E_{b,k}, E_{c,k}$ in the plane $\varphi = \psi/2$ and $E_{\varphi,k}$ perpendicular to this plane, while $B_{a,k}, B_{b,k}, B_{c,k}$ are allocated in the planes with $\varphi = 0$ resp. $\varphi = \psi$. The azimuthal magnetic flux components $B_{\varphi 1,k}$ and $B_{\varphi 2,k}$ are also allocated perpendicular to the plane $\varphi = \psi/2$ (compare Fig. 7).

Instead of presenting the difference equations (which can be found in detail in [25]) the following discrete representation of the induction

[1] This angle is arbitrary since all expressions in it may be shorted in the final equations.

law shall be given for the azimuthal order m:

$$\begin{pmatrix} -mI & 0 & 0 & -P_1 \\ 0 & mI & 0 & P_2 \\ 0 & 0 & mI & P_2 \\ I & P_3 & -I & 0 \\ P_4 & -I & I & 0 \end{pmatrix} \begin{pmatrix} e'_a \\ e'_b \\ e'_c \\ e'_\varphi \end{pmatrix} = \frac{\omega}{c} \begin{pmatrix} b'_a \\ b'_b \\ b'_c \\ b'_{\varphi 1} \\ b'_{\varphi 2} \end{pmatrix}$$

with the state variables e', b', the discrete curl operator C of the triangular grid and the block matrices[2]

$$P_1 = \begin{cases} -1 & \text{for} \quad k \\ +1 & \text{for} \quad k+1 \\ 0 & \text{else} \end{cases} ,$$

$$P_2 = \begin{cases} -1 & \text{for} \quad k \\ +1 & \text{for} \quad k+J \\ 0 & \text{else} \end{cases} ,$$

$P_3 = P_1 - I$, $P_4 = P_2 - I$, I being the unity matrix.

Correspondingly, Ampere's law and the two divergence equations can be discretized (cf. [31], [25] for details). Note that no sources and no driving currents are assumed.

The state variable d' is defined by $\int \epsilon_r \vec{E}' \cdot d\vec{A}$, the state variables b' hold $\int \mu_r \vec{H}' \cdot d\vec{A}$ (and not $\int \vec{B}' \cdot d\vec{A}$). This convention is in accordance with the field representation (2), (3).

The discrete curl operators C and $\tilde{C}$ and the discrete divergence operators S and $\tilde{S}$ obviously reflect the topology of the triangular (primary) grid and its dual grid and enumeration. The derivation of these operators is not as straightforward as in the case of a Cartesian grid treated in the previous section. The curl operator C of the primary triangular grid as given above and the curl operator $\tilde{C}$ of the dual hexagonal mesh fulfill the important property of a FIT curl operator:

$$C = \tilde{C}^T .$$

This generalized symmetry of the operators is basis for the consistency of FIT field solutions. The divergence operator is given here for the dual hexagonal grid:

$$\tilde{S} = (P_1^T | P_2^T | P_2^T | - mI)$$

[2] For sake of simplicity we regard a point $k = (j-1) \cdot J + 1$ in row j with j even (type I). For a point k of type II the indices may partially shift by ± 1. The detailed difference equations can be found in [31] and [25].

with the blocks P_i as given above.

Thus the *Maxwell-Grid-Equations* (1) for loss free time harmonic fields without driving current read as

$$\begin{aligned} Ce' &= kb' \\ \tilde{C}h' &= kd' \\ Sb' &= 0 \\ \tilde{S}d' &= 0 \end{aligned} \tag{4}$$

with the voltage vectors $e' = (e'_a, e'_b, e'_c, e'_\varphi)^T$, $h' = (h'_a, h'_b, h'_c, h'_{\varphi_1}, h'_{\varphi_2})^T$ and the flux vectors $d' = (d'_a, d'_b, d'_c, d'_\varphi)^T$, $b' = (b'_a, b'_b, b'_c, b'_{\varphi_1}, b'_{\varphi_2})^T$ in case that the electric field is allocated on the primary triangular grid. The components e'_a, e'_b, etc. themselves are vectors, e.g. $e'_a = (e'_{a,1}, ..., e'_{a,N})^T$, with the dimension N of numbers of grid points (compare Fig. 5). The factor $k = \omega/c$ stands for the wavenumber. Voltage and flux vectors are related via material operators which are build in full analogy to those described in section 1 of this paper.

In case of time harmonic fields the divergence equation is *automatically fulfilled* as was shown in [33]. Therefore it is possible to resolve the equation $\tilde{S}d' = 0$ for the azimuthal flux density d'_φ and substitute d'_φ resp. e'_φ in the remaining field equations. This formulation reduces the dimension of the system to be solved by the number of grid points N.

Finally, an algebraic eigenvalue problem

$$Ax = k^2 x$$

remains to be solved. Its eigenvalues are the squared wave numbers of the resonant frequencies, and the eigenvectors

$$x = (e'_{a,1}, ..., e'_{a,N}, e'_{b,1}, ..., e'_{b,N}, e'_{c,1}, ..., e'_{c,N})^T$$

give the corresponding electric voltages. Then, the magnetic fluxes are computed via the *Maxwell Grid Equations*. The eigenvalue problem is solved by some subspace method with polynomial acceleration described in [24] resp. [19]. The grid voltages are each connected to ten neighbouring grid voltages by the difference equations corresponding to the analytical 'curl curl − grad div' operation. The $(3N \times 3N)$-matrix A of the eigenvalue problem is sparse and the nonzero entries are located on a few off-diagonals, as shown in Fig. 8.

In case $m = 0$, i.e. for the so-called monopole modes, pure TE- and TM-modes can exist. For the TE0-modes with transverse electric field only the nonvanishing electromagnetic field components E_φ, H_r

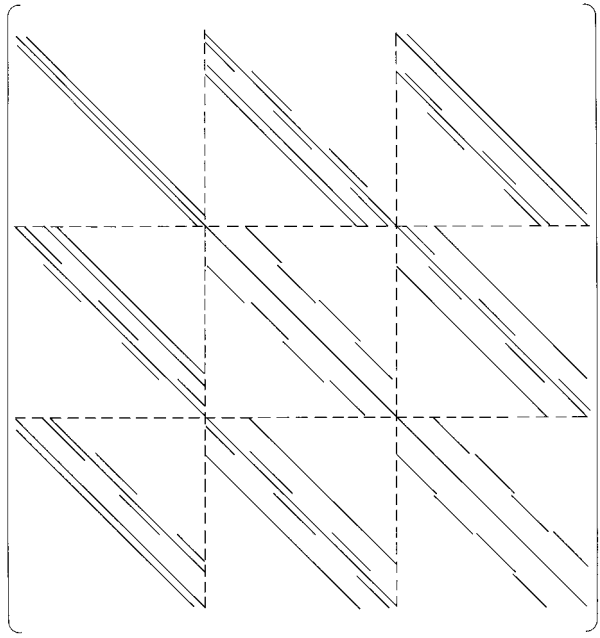

Figure 8. Matrix of the eigenvalue problem for $m > 0$.

and H_z have to be calculated while only H_φ, E_r and E_z have to be computed for the transverse magnetic TM0-modes. In this case less field components are related to each other which is expressed in a smaller matrix $(2N \times 2N)$ with less off-diagonals.

For structures with translational symmetry like longitudinally invariant waveguides, we have the longitudinal dependence

$$\vec{E}(x, y, z) = \vec{E}_0(x, y)e^{i\beta z},$$

which gives to a first approximation

$$\vec{E}(x, y, \Delta z) = \vec{E}_0(x, y)(1 + i\beta\Delta z),$$

with the propagation constant β.

Again, Maxwell's equations are discretized analogously to the case of modes with azimuthal order $m \geq 1$ in cylindrical symmetric cavities. Now, the longitudinal coordinate direction corresponds to the azimuthal coordinate. The resulting linear algebraic eigenvalue problem has the squared propagation constants β^2 for a given frequency ω as eigenvalues.

More details may be found in [31] and [26].

2.4. Error Behaviour

As shown in [31] the *discretization error* of URMEL-T follows the relation

$$\left|\frac{\Delta f}{f}\right| \propto \frac{1}{2.2 \cdot N^{1.2}}.$$

Regard some kind of model problem allowing to show the effect of a triangular mesh compared to a Cartesian mesh. The advantage of the triangular grid clearly becomes obvious in the reduced *geometric error* as Table 1 shows for a comparison with a Cartesian mesh: For the same number of unknowns, the relative error in frequency is one order smaller with the triangular grid.

Table 1. Lowest mode in a spherical cavity of 1m radius. The exact frequency is $f = 130.911$MHz [13]. Note that URMEL-T has twice the number of grid points as unknowns in case of monopole computations.

	Cartesian grid (URMEL)			triangular grid (URMEL-T)		
Mode	N	f/MHz	Error	2N	f/MHz	Error
TM0	121	128.972	$-1.5 \cdot 10^{-2}$	144	130.750	$-1.2 \cdot 10^{-3}$
EE-1	484	130.733	$-1.4 \cdot 10^{-3}$	576	130.879	$-2.4 \cdot 10^{-4}$
	1089	130.762	$-1.1 \cdot 10^{-3}$	1296	130.892	$+1.5 \cdot 10^{-4}$
	1936	130.655	$-2.0 \cdot 10^{-3}$	2232	130.885	$-2.0 \cdot 10^{-4}$
	3025	130.721	$-1.5 \cdot 10^{-3}$	3510	130.929	$+1.4 \cdot 10^{-4}$

2.5. Relation to Mixed Finite Elements

The key point in *consistent* discretization of Maxwell's equations is the need to use a pair of dual meshes. This is the breakthrough which was achieved in *mixed FEM* or *FEM with Whitney forms on a primal and dual mesh* (the notation is not unique for different authors), see e.g. [18, 14, 15, 4]. A key element in finding a synthesis between methods like FIT on the one hand and FEM with Whitney forms on the other hand is a diagonal Hodge operator [3].

Some important aspects of the procedure in context of a comparison between FIT and FEM are summarized following [22], [3]: In analogy to the discrete FIT-operators $S, C, ...$ the connectivity matrices on a simplicial mesh are discrete analogs to the divergence-, curl- and gradient-operator. The mass matrices of edge elements find some kind of analogy in the material operators $D_\varepsilon, \tilde{D}_\mu, D_\kappa$ of FIT. As shown in [22] the mass matrices can also be regarded as discrete analogs to the Hodge operator for differential forms. This terminology

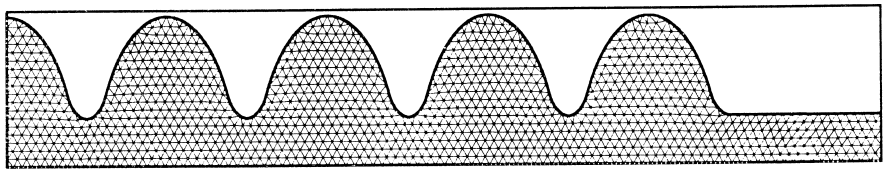

Figure 9. Triangular grid for multicell cavity.

comes from differential geometry. The Hodge operator maps p-forms to (n-p)-forms, i.e. for $n = 3$ and $p = 2$ it maps 2-forms to 1-forms. Concerning FIT, the state variables like d defined over surfaces may be regarded as 2-forms, while the other state variables like e defined along some path may be regarded as 1-forms and the material operators are some corresponding tensors.

Concerning FEM, the Galerkin method can be interpreted as a realization of the discrete Hodge operator [22]. A close link between FIT and mixed FEM may well be suspected, yet a theoretical interpretation from the point of view of differential geometry is still open for research.

3. EXAMPLES

In the previous section a first example was shown in Fig. 3: a loaded cavity. As many examples can be found in previous publications [29, 31, 30, 7, 8] only few simple examples will be shown here.

3.1. Tuned Multicell Cavity

The triangular grid is especially well suited for the tuning of multicell cavities. Figures 9 and 10 show the mesh and a plot of the field lines of $r \cdot H_\varphi$ at $\varphi = 0$ for the π-mode in the right half of a superconducting nine cell cavity. This TM0-mode has the frequency 1007 MHz. The radius of the inner cells is 139.595 mm. The last cell was tuned by 1.25 mm to a radius of 138.345 mm.

3.2. Dispersion Relation for Loaded Waveguide

A rectangular waveguide filled with some dielectrics [31] is shown in Fig. 11. Its fundamental mode has the frequency 3 GHz. The dispersion relation between frequency ω and propagation constant β has been computed. For different frequencies the highest β's are displayed in Fig. 12 in a fit through a few dozen distinct values. Note

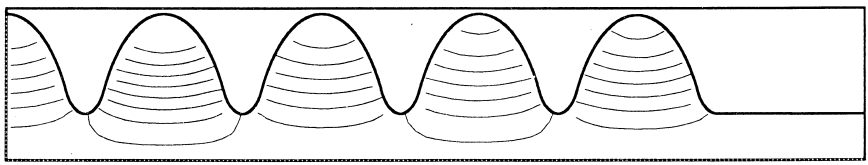

Figure 10. Contour plot of $r \cdot H_\varphi$ at $\varphi = 0$ for the π-mode in the nine cell cavity.

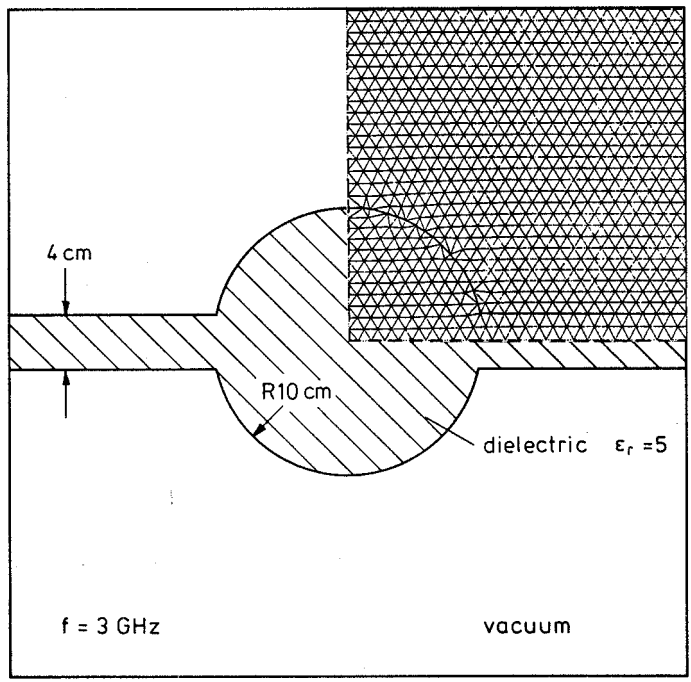

Figure 11. Dielectric waveguide with mesh for the part which only needs to be computed when exploiting all symmetries of the structure.

that for each wavenumber $k_0 = \omega/c$ one URMEL-T run has to be performed.

3.3. Circular Waveguide with Capacitive Load

The electric field lines of the TE_{11}-mode (H_{11}) in a circular waveguide with capacitive load are shown in Fig. 13. Its outer diameter is 10 cm. The cut off frequency is 580 MHz. Only a quarter of the

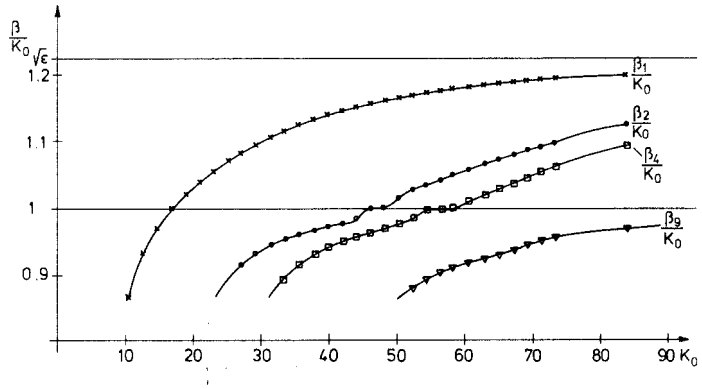

Figure 12. Dispersion relation for the dielectric-loaded waveguide.

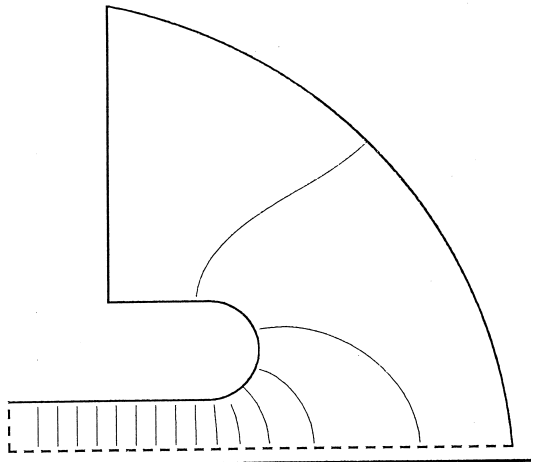

Figure 13. Electric field lines of the fundamental TE mode in a capacitively loaded circular waveguide at $f = 580$ MHz.

structure is discretized. The TE_{11}-mode can then be obtained by setting a magnetic boundary condition at one and an electric boundary condition at the other symmetry plane.

3.4. Parameter Study for Loaded Ridged Waveguide

Finally, a dielectric loaded ridged waveguide with post is shown which first has been computed in [7].

For this dielectric-slab-loaded ridged waveguide, shown in Fig. 14,

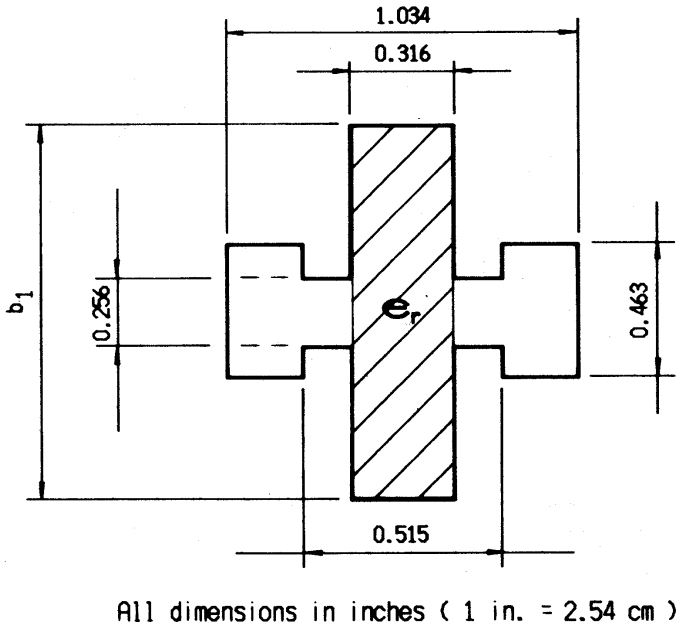

Figure 14. Geometry of dielectric-loaded ridged waveguide.

the effect of the slot height on guide parameters as the guide wavelength λ_g and the characteristic impedance Z_0, defined as

$$Z_0 = \frac{|V_0|^2}{2P_T},$$

where

$$V_0 = \int_{-b_1/2}^{b_1/2} E_y(0, y)dy$$

and

$$P_T = \frac{1}{2} \int \int_{Area} (\vec{E} \times \vec{H}^*) \cdot \hat{z} \; dxdy,$$

have been determined with URMEL–T and compared with mode matching results from [32]. Table 2 shows results for the case $\epsilon_r = 2.62 \cdot \epsilon_0$ and frequency $f = 5.95$ GHz. Evidently, the agreement with the semi-analytical results is very good.

Table 2. Effects of slot height on waveguide parameters.

	URMEL–T		Ref. [32]	
Slot Height b_1 / in.	λ_g / in.	Z_0/Ω	λ_g / in.	Z_0/Ω
0.256	1.7113	186	1.6983	178
0.300	1.7735	210	1.7634	203
0.350	1.8239	225	1.8192	224
0.450	1.8873	236	1.8872	252
0.650	1.9434	262	1.9320	270
0.850	1.9529	276	1.9404	274
1.056	1.9541	275	1.9411	274

4. CONCLUSION AND OUTLOOK

This paper revisited the application of the Finite Integration Technique on triangular grids. The corresponding code URMEL-T is successfully applied since more than 15 years in many different locations, mainly universities and accelerator laboratories. The underlying method has been described and some examples of cavity and waveguide computations were shown in this paper. A short hint on the analogies to FEM with Whitney forms on a primal and dual mesh was given. This point could be the onset of further research on a presumed equivalence of both methods.

REFERENCES

1. Bartsch, M., U. van Rienen, and T. Weiland, "Consistent finite integration approach for coupled computation of static current distributions and electromagnetic fields," *IEEE Trans. Magn.,* Vol. 34, No. 5, 3098–3101, Sept. 1998.
2. Bihn, M. and T. Weiland, "A Stable discretization scheme for the simulation of elastic waves," *15th IMACS World Congress on Scientific Computation, Modelling and Applied Mathematics,* Vol. 2, 75–80, Berlin, 1997.
3. Bossavit, A., private communication.
4. Bossavit, A., *Computational Electromagnetism, Variational Formulations, Edge Elements, Complementarity,* Academic Press, Boston, 1998.
5. Clemens, M., R. Schuhmann, U. van Rienen, and T. Weiland, "Modern Krylov subspace methods in electromagnetic field

computation using the finite integration theory," *ACES Journal, Special Issue on Applied Mathematics: Meeting the Challenges Presented by Computational Electromagnetics,* Vol. 11, No. 1, 70–84, March 1996.

6. Clemens, M., P. Thoma, T. Weiland, and U. van Rienen, "A survey on the computational electromagnetic field calculation with the FI method," *Surveys on Mathematics for Industry,* Vol. 8, No. 3–4, 213–232, 1999.
7. Cooper, R. K., M. J. Browman, T. Weiland, and U. van Rienen, "Waveguide calculations using established codes," *IEEE Trans. Electron Devices,* Vol. 35, No. 11, 2044–2047, 1988.
8. Cooper, R. K., U. van Rienen, and T. Weiland, "RF waveguide design by proven electromagnetic CAD systems," *General Assembly of the URSI,* Israel, Tel Aviv, August 1987.
9. Dehler, M., "Numerische lösung der Maxwellschen Gleichungen auf kreiszylindrischen gittern," Ph.D. thesis, Darmstadt University of Technology, 1993.
10. Dehler, M. and T. Weiland, "A new spectral domain technique for the calculation of eigenvalues in curvilinear coordinates," *IEEE Trans. Magn.,* Vol. 30, No. 5, 3574–3577, 1994.
11. Dohlus, M., P. Thoma, and T. Weiland, "Stability of finite difference time domain methods related to space and time discretization," *IEEE Trans. Microwave Theory Tech.,* submitted.
12. Fellinger, P., "Ein Verfahren zur numerischen lösung elastischer wellenausbreitungsprobleme im zeitbereich durch direkte diskretisierung der elastodynamischen grundgleichungen," Ph.D. thesis, Gesamthochschule Kassel, 1991.
13. Henke, H., *Spherical Modes,* ISR-RF 81-29, CERN, Geneva, Switzerland, 1981.
14. Nédélec, J., "Mixed finite elements in R^3," *Numer. Math.,* Vol. 35, 315–341, 1980.
15. Nédélec, J., "A new family of mixed finite elements in R^3," *Numer. Math.,* Vol. 50, 57–81, 1986.
16. Pinder, P., "Zur numerischen berechnung gekoppelter elektromagnetischer und thermischer felder," Ph.D. thesis, Darmstadt University of Technology, 1998.
17. Pinder, P. and T. Weiland, "Numerical calculation of coupled electromagnetic and thermal fields using the finite integration method," *PIERS'96,* 1996.
18. Raviart, P.-A. and J.-M. Thomas, "A mixed finite element

method for second order elliptic problems," *Mathematical Aspects of the Finite Element Method,* I. Galligani and E. Magenes (eds.), 292–315. Springer-Verlag, 1977.

19. Schmitt, D. and T. Weiland, "2D and 3D computations of eigenvalue problems," *IEEE Trans. Microwave Theory Tech.,* Vol. 28, No. 2, 1793–1796, 1992.
20. Schuhmann, R. and T. Weiland, "Stability of FDTD algorithm on nonorthogonal grids related to the spatial interpolation scheme," *IEEE Trans. Microwave Theory Tech.,* Vol. 34, No. 5, 2751–2754, Sept. 1998.
21. Schuhmann, R. and T. Weiland, "A stable interpolation technique for FDTD on nonorthogonal grids," *Int. J. Numerical Modelling, Focused Issue on "Finite Difference Time and Frequency Domain Methods",* Vol. 11, 299–306, 1998.
22. Tarhasaari, T., L. Kettunen, and A. Bossavit, "An interpretation of the Galerkin method as the realization of a discrete hodge operator," *8th Biennal IEEE Conf. on Electromagnetic Field Computation CEFC 1998,* Tucson, Arizona, USA, June 1998.
23. Thoma, P. and T. Weiland, "A consistent subgridding scheme for the finite difference time domain method," *Int. J. Numerical Modelling,* Vol. 9, 359–374, 1996.
24. Tückmantel, J., *Application of SAP in URMEL,* EF/RF 85-4, CERN, Geneva, Switzerland, July 1985.
25. van Rienen, U., "Zur numerischen Berechnung zeitharmonischer elektromagnetischer felder in offenen, zylindersymmetrischen strukturen unter verwendung von mehrgitterverfahren," Ph.D. thesis, Darmstadt University of Technology, 1989.
26. van Rienen, U., "Finite integration technique on triangular grids revisited," *Int. J. Numerical Modelling: Electronic Networks, Devices and Fields, Special Issue "Finite Difference Time and Frequency Domain Methods",* Vol. 12, 107–128, 1999.
27. van Rienen, U., *Numerical Methods in Computational Electrodynamics - Linear Systems in Practical Applications,* Vol. 12 of *Lecture Notes in Computational Science and Engineering,* Springer, 2000.
28. van Rienen, U., P. Pinder, and T. Weiland, "Consistent finite integration approach for the coupled calculation of electromagnetic fields and stationary temperature distributions," In *7th Biennal IEEE Conference on Electromagnetic Field Computation (CEFC),* 294, Okayama, Japan, March 1996.
29. van Rienen, U. and T. Weiland, "Triangular discretization

method for the evaluation of RF-fields in cylindrically symmetric cavities," *IEEE Trans. Magn.,* Vol. 21, No. 6, 2317–2320, November 1985.

30. van Rienen, U. and T. Weiland, "Cavity and waveguide design by triangular mesh code URMEL-T," *Int. Linear Accelerator Conf. LINAC'86,* No. SLAC-303, 286, Stanford University, June 1986.
31. van Rienen, U. and T. Weiland, "Triangular discretization method for the evaluation of RF-fields in waveguides and cylindrically symmetric cavities," *Part. Acc.,* Vol. 20, 239–267, 1986/87.
32. Villeneuve, A. T., "Analysis of slotted, dielectrically loaded, rigded waveguide," *IEEE Trans. Microwave Theory Tech.,* Vol. 32, 524–532, 1984.
33. Weiland, T., "Eine methode zur lösung der Maxwellschen Gleichungen für sechskomponentige felder auf diskreter basis," *Archiv für Elektrotechnik,* Vol. 31, 116–120, 1977.
34. Weiland, T., "Zur berechnung der wirbelströme in beliebig geformten, lamellierten, dreidimensionalen eisenkörpern," *Archiv für Elektrotechnik,* Vol. 60, 345–351, 1978.
35. Weiland, T., "On the unique numerical solution of Maxwellian Eigenvalue problems in three dimensions," *Part. Acc.,* Vol. 17, 227–242, 1985.
36. Weiland, T., "Ein allgemeines verfahren zur lösung der Maxwell'schen Gleichungen und seine anwendung in physik und technik," *Physikalische Blätter,* Vol. 41, 380, 1986.
37. Weiland, T., "Elektromagnetisches CAD — rechnergestützte methoden zur berechnung von feldern," Script, Darmstadt University of Technology, May 1995.
38. Weiland, T., "High precision eigenmode computation," *Part. Acc.,* Vol. 56, 61–82, 1996.
39. Wolter, H., "Berechnung akustischer wellen und resonatoren mit der FIT-methode," Ph.D. thesis, Darmstadt University of Technology, 1995.
40. Yee, K. S., "Numerical solution of initial boundary value problems involving Maxwell's equations in isotropic media," *IEEE Trans. Antennas Propagat.,* Vol. 14, 302–307, 1966.